

Chapter 7:
Distinct Element Models for the Coupled T-M-H
Processes: The Theory Implementation

CHAPTER 7

Distinct Element Models for the Coupled T-H-M Processes: Theory and Implementation

Mikko P. Ahola^a, Asadul H. Chowdhury^a, and Alain Thoraval^b

^aCenter for Nuclear Waste Regulatory Analyses, Southwest Research Institute, 6220 Culebra Road, San Antonio, TX, 78238, USA

^bLaboratoire de Mecanique des Terrains, Institut National de L'Environnement Industriel et des Risques, Parc de Saurupt (INERIS), 54042, Nancy, France

7.1 INTRODUCTION

In the case of a fractured rock medium where the discontinuities play a critical role in determining the deformation and rigid body motion (Kana et al., 1991; Hsiung et al., 1992a,b), the distinct element method (DEM) (Cundall and Hart, 1985; Applied Mechanics Inc., 1985; Itasca, 1992; Cundall et al., 1978; Cundall, 1971; Itasca, 1989; Hart et al., 1988; Williams and Mustoe, 1987) which uses the discontinuum modeling technique is a rational method for modeling the medium. In this method, properties of both the joints and the intact rocks are explicitly modeled. This is in contrast to continuum methods such as finite element (Zienkiewicz and Morgan, 1983) and finite difference (Forsythe and Wasow, 1960) which, in most cases, homogenize the properties of joints and intact rock into a pseudocontinuum. The DEM has two distinguishing features compared to continuum methods: (i) the behavior of the geologic system is described by both a continuum material description of the intact rock and a discontinuum material representation for discontinuities (i.e., joints, faults, etc.), and (ii) the deformation mechanisms include large displacement (i.e., joint slip and separation) and block rotation. In both the DEM and the continuum methods, the problem domain is discretized into a system of solid elements (blocks). However, in the DEM, the geometry of the blocks is generally constrained by the spacing and orientation of the discontinuities in the rock mass, thereby allowing blocks to interact with (or disconnect from) neighboring blocks. The DEM includes not only continuum theory representation for the blocks but also force-displacement laws which specify forces between blocks and motion law which specifies motion of each block due to unbalanced forces acting on the block.

Blocks may be treated as rigid or deformable in the DEM. The rigid block formulation (Cundall, 1971) represents the medium as a set of distinct blocks bounded by the joints in which the blocks do not change their individual geometries as a result of applied loading and only the joints can deform (i.e., the blocks move relative to each other) (Itasca, 1989). Consequently, the formulation is most applicable to problems in which behavior of the system is dominated by discontinuities and where the material elastic properties may be ignored. Such conditions arise in low-stress environments and/or where the individual blocks

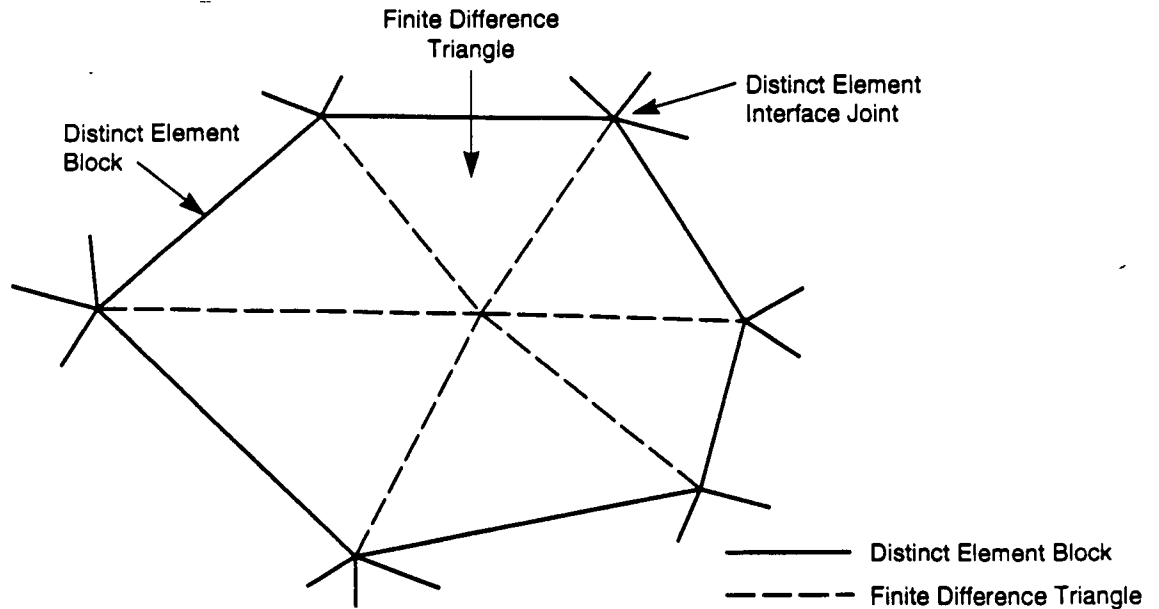


Figure 7.1. Internal discretization of distinct element block into finite difference triangles.

The DEM is a subclass under the more general heading of discrete element (discontinuum) methods, which consist mainly of the (i) DEM, (ii) modal method, (iii) discontinuous deformation analysis method, and (iv) momentum exchange method (Chowdhury et al., 1992). Programs based on the DEM (e.g., UDEC (Cundall, 1980; Itasca, 1992) and 3DEC (Hart et al., 1988; Itasca, 1990) use an explicit, time-marching scheme to solve directly the equations of motion. As discussed earlier, bodies may be rigid or deformable, and the contacts are taken to be deformable. The modal method is similar to the DEM in the case of rigid bodies, but for deformable bodies, modal superposition is used (Williams and Mustoe, 1987). In the discontinuous deformation analysis, contacts are rigid and bodies may be rigid or deformable. The condition of no-interpenetration is achieved by an iteration scheme. The body deformability is implemented by superposition of strain modes (Shi and Goodman, 1988). Finally, in the momentum exchange method both contacts and the bodies are rigid; momentum is exchanged between two contacting bodies during an instantaneous collision (Hahn, 1988).

Of the four types of discrete element methods identified above, the literature indicates that only the DEM has made significant progress toward adding thermal and hydrological capabilities to mechanical analysis capabilities and consequently will be the method focused on in this chapter. In codes utilizing the DEM (e.g., UDEC), the equations governing the mechanical, thermal, and hydrologic response are not fully coupled. Rather, the coupling is achieved within the solution process in which explicit or implicit time marching is done on one process while the other is held fixed, and vice versa. For mechanical processes, the governing equations are the equations of motion, while for

Development of the DEM can be divided into the following three major phases: (i) modeling of jointed rigid blocks, (ii) modeling of simply deformable discontinua, and (iii) modeling of fully deformable discontinua. Modeling jointed rigid blocks was originally proposed in a restricted form by Cundall (1971) which was later generalized by Cundall (1974) and Cundall et al. (1978). It was developed for low-stress rock situations where displacement due to joints far exceeds those of the intact rock blocks. The main assumption in this approach is that the rock is rigid and only the joints can deform. A joint is regarded as a boundary interaction between two blocks and is not represented as a separate element. Joint properties may be specified with very general force-displacement relationships which are possible in both the normal and shear directions. However, the underlying assumption is that the compressive normal stiffness of a joint is very large compared to the joint shearing stiffness and the tensile normal stiffness of the joint, i.e., the process of failure is brought about by joint shearing or tensile separation.

Modeling jointed rigid blocks assumes that the geometry of block boundaries is not changed by pressure between blocks in the normal direction and that normal force between blocks is proportional to the linear overlap (Cundall, 1971) between blocks. As a result, this formulation may not satisfy the compatibility of compression deformation of the two blocks at the contact point, although deformation at the contact point may be small due to high compressive normal stiffness of the joint.

Although in this modeling approach there is no limit to the amount of displacement or rotation allowed for each block, its incremental response calculation is based on the small incremental displacement within the time step. DEM uses the explicit time discretization and, thereby, keeps the time step very small; i.e, smaller than some critical value which is a function of the mass and stiffness of the rock components. However, care should be exercised because the use of a small time step may not guarantee small displacement within the time step, especially when elasto-plastic force-displacement relationships are used for joint properties,

Modeling of simply deformable discontinua is an enhancement over modeling jointed rigid blocks. Modeling the geologic medium as simply deformable discontinua is suitable for representing rock systems where the rock matrix behavior, although affecting the mechanics of the system, does not participate strongly enough for the more complex deformation modes to contribute much of the overall deformation. This model gives, for example, each two-dimensional block three degrees of freedom to deform internally, in addition to the three rigid-body models already associated with each rock block of a jointed rigid block model. The simplifications embodied in modeling simply deformable discontinua are only concerned with the number of degrees of freedom associated with rock block deformations. Constitutive laws of the rock blocks can be completely general and include plasticity and arbitrary nonlinear behavior.

$$\ddot{u} = \frac{\dot{u}^{(t+\Delta t/2)} - \dot{u}^{(t-\Delta t/2)}}{\Delta t} \quad (7.2)$$

A difference equation equivalent to (7.1) can be written as:

$$\frac{\dot{u}^{(t+\Delta t/2)} - \dot{u}^{(t-\Delta t/2)}}{\Delta t} = \frac{F^{(t)}}{m} - \alpha \left[\frac{\dot{u}^{(t+\Delta t/2)} + \dot{u}^{(t-\Delta t/2)}}{2} \right] + g \quad (7.3)$$

Note that the damping force in the equation is centered at time t .

Rearranging Eq. (7.3) yields:

$$\dot{u}^{(t+\Delta t/2)} = \left[\dot{u}^{(t-\Delta t/2)} \left(1 - \frac{\alpha \Delta t}{2} \right) + \left(\frac{F^{(t)}}{m} + g \right) \Delta t \right] / (1 + \alpha \Delta t/2) \quad (7.4)$$

With velocities stored at the half-timestep point, it is possible to express displacement as:

$$u^{(t+\Delta t)} = u^{(t)} + \dot{u}^{(t+\Delta t/2)} \Delta t \quad (7.5)$$

Because the force depends on displacement, the force-displacement calculation is done at one time instant. The acceleration is also given by the force at this time instant (i.e., $t+\Delta t$) and the mass. Figure 7.2 illustrates the central difference scheme with the order of calculation indicated by the arrows.

For blocks which are acted upon by several forces as well as gravity, the velocity equations become:

$$\dot{u}_i^{(t+\Delta t/2)} = \left[\dot{u}_i^{(t-\Delta t/2)} \left(1 - \frac{\alpha \Delta t}{2} \right) + \left(\frac{\sum F_i^{(t)}}{m} + g_i \right) \Delta t \right] / (1 + \alpha \Delta t/2) \quad (7.6)$$

where \dot{u}_i = velocity components of centroid in i th direction
 $\sum F_i^{(t)}$ = summation of forces acting on centroid in i th direction

Similiary, the equation of motion for rotation is given by:

$$u_i^{(t+\Delta t)} = u_i^{(t)} + \dot{u}_i^{(t+\Delta t/2)} \Delta t \quad (7.9)$$

$$\theta^{(t+\Delta t)} = \theta^{(t)} + \dot{\theta}^{(t+\Delta t/2)} \Delta t \quad (7.10)$$

where θ = rotation of block about centroid, and
 u_i = coordinates of block centroid

Thus, each iteration produces new block positions which generate new contact forces. Resultant forces and moments are used to calculate linear and angular accelerations of each block. Block velocities and displacements are determined by integration over incremental timesteps. The procedure is repeated until a satisfactory state of equilibrium or mode of failure results.

7.2.1.3 Explicit Solution Procedure

The DEM is based on an explicit solution procedure (Itasca, 1992). "Explicit" refers to the nature of algebraic equation used in the numerical simulation of the physical system. In the explicit method, all quantities on one side of all equations are known, and each equation is simply evaluated to produce the result on the other side of the equation. Explicit formulations differ from implicit formulations, where unknown quantities exist on both sides of the equation; implicit formulations require the solution of simultaneous equations by some technique such as transpose elimination or Gauss elimination.

The explicit formulation relies on the fact that it takes a finite time for effects to propagate through a system of blocks. The interdependence of variables over a selected time interval may be neglected if the time interval is small enough for effects to pass between neighboring blocks at a speed greater than physically possible. In other words, the numerical procedure is stable when the equations of motion for all blocks become uncoupled by selecting a time interval between subsequent integration intervals which is smaller than that required for adjacent blocks to communicate physically. The small timestep is the main disadvantage of the explicit method. Determination of the required timestep is based on block masses and stiffnesses present in the problem. An advantage of the explicit method is that, because matrices are never formed, large displacements and non-linear or post-elastic behavior are possible with no additional computing effort.

7.2.1.4 Interface Constitutive Relations

The deformability of the discontinuities or interface between blocks and the frictional characteristics are represented in the DEM by spring-slider systems with prescribed force-displacement relations which allow evaluation of shear and normal forces between blocks (Itasca, 1992). In the model, spring-slider systems are located at contact points between

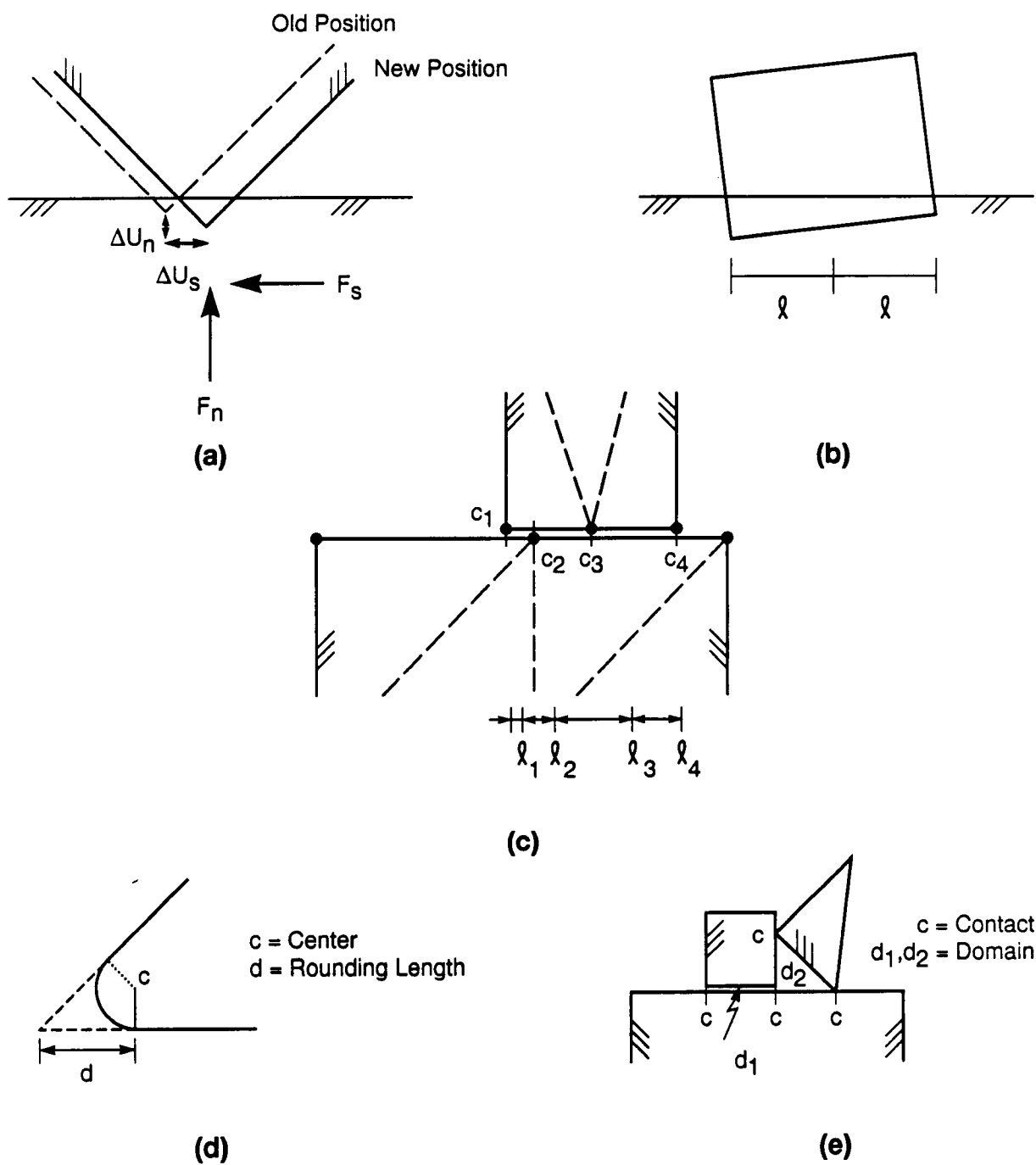


Figure 7.4. Block contact geometry: (a) corner-edge contact; (b) edge-edge contact; (c) contact lengths for fully deformable blocks; (d) rounding corner; and (e) domains.

where τ_o is shear strength of the joint, σ_n is normal stress across the joint, C is cohesion, and ϕ is friction angle. Once τ_o is reached, the joint assumes a perfectly plastic deformation. This equation suggests that the shear strength of a joint is the same in all directions. The joint shear response is governed by a constant shear stiffness k_s ,

$$\Delta\tau = k_s \Delta u_s^e \quad (7.16)$$

where $\Delta\tau$ is incremental shear stress and Δu_s^e is an elastic component of the incremental shear displacement. Based on Eqs. (7.15) and (7.16), $\Delta\tau$ becomes zero after the condition $|\tau| = \tau_o$ is reached, where τ is the shear stress on the joint. There is also a limiting tensile strength of the joint. If the tensile stress across the joint exceeds this value, the joint fails in tension and σ_n equals zero.

The Mohr-Coulomb joint model in its basic form does not consider joint wear and dilation behavior. However, the dilation behavior may be added to the joint behavior (Itasca, 1992). In UDEC, dilation is restricted such that the dilation angle ψ is zero until shear stress has reached the shear strength of the joint; that is, joint dilation starts after the joint begins to deform plastically. A constant dilation angle is assumed for joint dilation, which returns to zero after a critical shear displacement is reached. Mathematically, the relation is (Itasca, 1992):

$$\text{if } |\tau| < \tau_o, \text{ then } \psi = 0 \quad (7.17)$$

and

$$\text{if } |\tau| = \tau_o \text{ and } |u_s| \geq u_{cs}, \text{ then } \psi = 0 \quad (7.18)$$

where u_s is the joint shear displacement and u_{cs} is the critical shear displacement. Eq. (7.18) suggests that joint dilation should continue to increase even during reverse shearing (Itasca, 1992).

7.2.1.6 Barton-Bandis Model

The Barton-Bandis model was proposed to take into consideration the effect of various joint material properties as well as applied normal loading on joint deformation and strength. The nonlinear joint strength criterion can be expressed as (Barton et al., 1985)

$$\tau_o = \sigma_n \tan \left[JRC \log_{10} \left(\frac{JCS}{\sigma_n} \right) + \phi_r \right] \quad (7.19)$$

where JRC is joint roughness coefficient, JCS is joint wall compressive strength, and ϕ_r is residual joint friction angle. Attrition of the surface roughness or reduction of the JRC is represented in a piece-wise linear manner as shown in Figure 7.5. The table in the figure

reduced from JRC_{peak} to JRC_f . If, at this point, the direction of the shear is reversed, the initial shear stress required for the joint to be sheared in the opposite direction is controlled by the JRC_f value, following Eq. (7.19), which serves as the maximum JRC in the reverse direction. In other words, the Barton-Bandis model assumes that the shear strength at the initiation of shear in the reverse direction is equal to the shear strength right before the forward shearing stopped. Also, the data in the inset table in Figure 7.5 suggest that joint wear will stop after the JRC_{mob} becomes zero. This condition will be reached when the ratio of the actual shear displacement δ to the shear displacement δ_p is greater than 100. Once the JRC becomes zero, the joint shear essentially resumes the Coulomb model type of behavior.

The Barton-Bandis joint model (Barton et al., 1985) also recognizes the dilation of joints and suggests that the angle of dilation should be a function of JRC value. The relation between the JRC and dilation angle ψ can be expressed in the following form

$$\psi = 0.5 JRC \log_{10} \left(\frac{JCS}{\sigma_n} \right) \quad (7.21)$$

This equation indicates that, as joint surface roughness wears, its angle of dilation decreases. In other words, the rate of dilation becomes smaller as joint shearing progresses. The dilation angle will eventually become zero, that is, there will be no further dilation as δ/δ_p becomes greater than 100. Judging from the nature of Eq. (7.21), ψ is always positive. Joint dilation will continue to increase, although at a gradually slower rate, even after the direction of shear has been reversed.

7.2.1.7 Continuously-Yielding Model

Numerical modeling of practical problems may take the joints through rather complex load paths. Many empirical models only provide the response to simple loading conditions. More general situations require either interpolation between curves or other arbitrary assumptions. The Continuously-Yielding model (Cundall and Hart, 1984; Hart et al., 1988; Itasca, 1992) is intended to simulate the intrinsic mechanism of progressive damage of the joint under shear. The model provides continuous hysteretic damping for dynamic simulations.

The response of a joint to normal loading is expressed incrementally as

$$\Delta \sigma_n = k_n \Delta u_n \quad (7.22)$$

where k_n is the normal stiffness of the joint, given by $k_n = a_n \sigma_n^{e_n}$, representing the observed increase of stiffness with normal stress, where a_n and e_n are model parameters. In general, zero tensile strength is assumed.

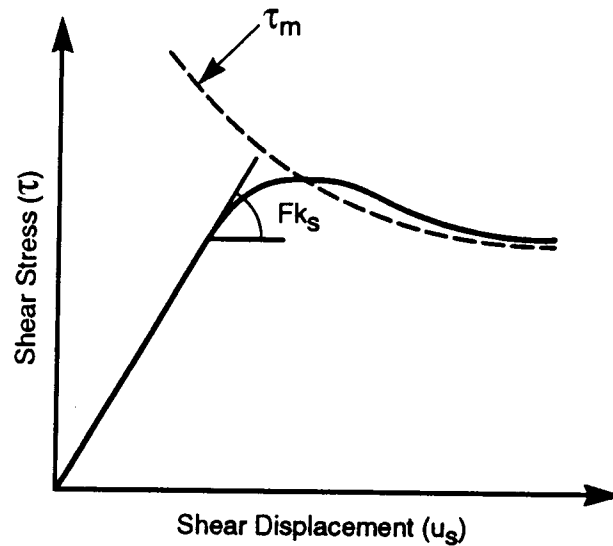


Figure 7.6. Continuously-Yielding joint model shear stress-displacement curve and bounding shear strength [after Cundall and Hart (1984)].

$$\phi_m = (\phi_{m0} - \phi) \exp \left[-\frac{u_s^r}{R} \right] - \phi \quad (7.29)$$

where u_s^P is the plastic shear displacement and the plastic shear displacement increment Δu_s^P is given by

$$\Delta u_s^P = (1 - F) |\Delta u_s| \quad (7.30)$$

and ϕ is the basic friction angle of the rock surface. R is a material parameter with a dimension of length that expresses the joint roughness. A large value of R produces slower reduction of ϕ_m and a higher peak. The peak is reached when the bounding strength equals the shear stress. After the peak, the joint is in the softening region and the value of F becomes negative.

Based on Eq. (7.28), joint bounding shear strength under a constant normal stress condition depends solely on the friction angle, ϕ_m . If a joint is sheared in one direction and its friction angle ϕ_m is reduced from its initial value ϕ_{m0} to ϕ_f ; then at this point, if the direction of the shear is reversed, the corresponding bounding shear strength in the reversed direction, is controlled by the ϕ_f . In other words, the Continuously-Yielding model assumes that the maximum bounding shear strength during reverse shearing is the same as the bounding shear strength at the end of the forward shearing process.

The formulation of joint dilation angle in the Continuously-Yielding model is expressed as (Hart et al., 1988)

$$\Delta \tau_{ij}^e = \lambda \Delta \epsilon_v \delta_{ij} + 2\mu \Delta \epsilon_{ij} \tag{7.35}$$

where λ , and μ are the Lamé's constants,

$\Delta \tau_{ij}^e$ = are the elastic increments of the stress tensor

$\Delta \epsilon_{ij}^e$ = are the incremental strains

$\Delta \epsilon_v$ = $(\Delta \epsilon_{11} + \Delta \epsilon_{22})$ is the increment of volumetric strain in two dimensions, and

δ_{ij} = Kronecker delta function

7.2.1.9 Calculation Sequence

The calculations performed in the DEM (e.g., UDEC) alternate between application of a force-displacement law at the contacts and Newton's second law of motion at the blocks. The force-displacement law is used to find contact forces from displacements. Newton's second law gives the motion of the blocks resulting from the forces acting on them. If the blocks are deformable, motion is calculated at the gridpoints of the triangular finite-difference (constant-strain) elements within the blocks. Then, the application of the block material constitutive relations gives new stresses within the elements. Figure 7.7 shows schematically the calculation cycle for the DEM.

This numerical formulation conserves momentum and energy by satisfying Newton's laws of motion exactly. Although some error may be introduced in the computer programs by the numerical integration process, this error may be made arbitrarily small by the use of suitable timesteps.

7.2.2 Hydrologic Behavior

In many cases hydrologic flow through rock masses has been observed both in the laboratory and field to be fracture dominated (Nitao et al., 1992). As the fractures or discontinuities in a rock mass will be several orders of magnitude more permeable than the rock matrix itself, the flow of fluid in a saturated rock mass can be expected to be concentrated along the discontinuities. Thus, in distinct element formulations it is reasonable to consider explicitly only fluid flow within the fractures, as is the case with UDEC. Flow of fluid in an unsaturated rock mass may not be dominated by fractures, depending on the infiltration, since the matrix suction (potential) would cause the fluid to avoid large pores/fractures.

Flow in planar rock fractures is idealized as laminar viscous flow between parallel plates. In this model, the flow rate per unit width, q , is given by

$$q = C a^3 \left[\frac{\Delta p}{l} \right] \tag{7.36}$$

$$C = \frac{1}{12\mu} \tag{7.37}$$

where C is the fluid flow joint property which is assumed to remain constant

- a is the joint hydraulic aperture
- μ is the dynamic viscosity of the fluid
- Δp is the change in pressure across a contact between adjacent domains, and
- l is the length assigned to the contact (see Figure 7.4)

The joint permeability can be defined as $K = \frac{ga^2}{12\nu}$ where g is the acceleration due to gravity, ν is the kinematic viscosity of the fluid.

The rate of fluid flow thus is assumed to be dependent upon the cubic power of the aperture. In actual rock fractures, the fracture walls are far from smooth and Eq. (7.36) does not truly represent the real case. The effect of roughness may cause a reduction in flow from that predicted using (Eq. 7.36), however, this can be accounted for by applying an empirical correction factor to Eq. (7.36) to account for fracture roughness (Louis, 1969). Witherspoon et al. (1980) tested both open and closed joints and concluded that the cubic law is still valid for the latter, provided that the actual mechanical aperture is used.

7.2.3 Thermal Behavior

Heat transfer can take place through either conduction, convection, or radiation. Convection can take place within the rock mass via groundwater flow and redistribution due to gravity, heating, or other mechanisms. This is discussed in more depth in Section 7.3.3. Convection may also take place from a surface of, for example, a tunnel or waste canister as a result of air circulation. Thermal radiation heat transfer can be the dominant heat transfer mechanism from solid surface to solid surface within a spent fuel assembly (Manteufel, 1991) and perhaps also important from the waste package to the surrounding borehole rock as well as across tunnel openings (e.g., from hot floor to cool roof) depending on whether the borehole/tunnel is backfilled or not. Within the rock medium, depending on amount of fluid movement within the fractures, conductive heat transfer most often dominates. It has been observed in studies that the existence of fractures can have some effect on conductive heat transfer through the rock by lowering the thermal conductivity (Sandford et al., 1984). However, such thermal properties (e.g., thermal conductivity and specific heat), can have a

if k_x and k_y are constant. This is the standard two-dimensional heat diffusion equation.

The method suggested by St. John (1985) can be applied to determine the radius of influence of a single heat source or waste container on rock temperatures as a function of time in order to determine the size of the area required in a model for heat transfer analysis. The equation for temperature change at a distance, R_o , from a decaying point source of initial strength, Q_o , is given by Christianson (1979)

$$\Delta T = \frac{Q_o}{\pi^{3/2}} \exp(-At) \frac{\sqrt{\pi}}{4\kappa} \exp(-R_o^2/4\kappa t) \operatorname{Re} \left[w \left(\sqrt{At} + \frac{iR_o}{\sqrt{4\kappa t}} \right) \right] \quad (7.42)$$

where i = imaginary number $\sqrt{-1}$
 A = thermal constant
 κ = thermal diffusivity
 t = time (s)
 $w(z)$ = complex error function in which z is the complex argument
 $\operatorname{Re}()$ = real part of argument

It is seen that the temperature change decays from the point source approximately proportional to

$$\exp(-R_o^2/4\kappa t) \quad (7.43)$$

St. John (1985) suggested that $R_o^2/4\kappa t = 4$ is sufficient to ensure a small temperature change. This expression requires that

$$R_o \geq 4\sqrt{\kappa t} \quad (7.44)$$

where t is time in years.

7.3 COUPLED PROCESSES

The response of a rock mass in a high-level nuclear waste (HLW) geologic repository, geothermal reservoir, etc. is a coupled phenomenon involving thermal (T), mechanical (M), hydrological (H), and chemical (C) processes (Wang et al., 1983; Tsang, 1987a,b; 1991; Manteufel et al., 1993). Coupled processes imply that one process affects another and that rock mass response in a repository environment cannot be predicted by considering each process independently. The importance of various processes will depend upon the thermal loading of the repository, the design of the engineered barriers, properties

δ_{ij}	=	Kronecker delta function
K	=	bulk modulus (N/m ²)
β	=	volumetric thermal expansion coefficient (1/°C), and
ΔT	=	temperature change

Note that $\beta = 3\alpha$, where α is the linear thermal expansion coefficient.

Equation (7.45) assumes a constant temperature in each triangular zone which is interpolated from the surrounding gridpoints. The incremental change in stress is added to the zone stress state prior to application of the constitutive law. The procedure for running a coupled thermomechanical simulation is shown in Figure 7.8. The fundamental requirement in performing the simulation is that temperature increases between successive thermal timesteps cause only "small" out-of-balance forces in blocks. Out-of-balance forces are small if they do not adversely affect the solution. For nonlinear problems, some experimentation may be necessary to obtain a sense of what small means in the particular problem being solved. This is performed by trying different allowable temperature increases when running the problem.

7.3.2 Two-Way Hydro-Mechanical Analysis for Fluid Flow in Fractured Media

Mechanical processes can affect the flow of fluids in the rock mass by changing the joint aperture and the bulk porosity of the rock matrix. Changes in aperture, in turn, would change the permeability of the joints. The change in joint aperture may be due to both normal and shear displacements of the joints. Shear displacement causes dilation which increases the joint aperture. The aperture of a joint also increases with the decrease of normal stress acting on it.

Creation of an opening in the rock mass redistributes the *in situ* stress field. Stress concentration around the excavation changes the apertures of the existing joints. Seismic loading from earthquakes can also change the aperture of the joints. Change in apertures not only changes the hydraulic conductivities of the rock but may also change the preferential flow path.

Rock mass may fail due to displacements along the joints. Depending on the strength of the rock, additional fractures can form which also change the hydraulic conductivities of the rock mass surrounding the excavations. The method of excavation can create additional fractures in the surrounding rock. These fractures reduce the load-bearing capacity and increase the bulk hydraulic conductivities of the rock mass.

The state of stress in a rock mass is coupled to the flow of groundwater. Presence of fluid in the rock can also change the mechanical properties. In unconfined compression tests (Olsson and Jones, 1980), saturated samples of Grouse Canyon tuff, a volcanic rock located at the Nevada Test Site, are 24 percent weaker than dry samples. Presence of water

$$V_m = (V + V_o)/2$$

For small joint apertures the fluid appears to be a stiff spring, with a stiffness higher than the typical joint stiffness. In an explicit algorithm, this implies that the mechanical timestep must be reduced. The fluid timestep, which is calculated by

$$\Delta t_f = \min \left[\frac{V}{K_w \sum_i K_i} \right] \tag{7.47}$$

where V is the domain volume and the summation of permeability factors K_i is extended to all contacts surrounding the domain, is inversely proportional to the bulk modulus and joint conductivity. For typical joint apertures, fluid timesteps on the order of milliseconds are obtained. Therefore, this current UDEC algorithm can only be applied to short-duration simulations.

A new procedure was developed that appears to overcome the difficulties described in the preceding discussion. Before presenting this scheme, it is worthwhile to review the essential characteristics of a fluid-rock system and the particular conditions to be modeled. The characteristics of a rock-fluid system can be summarized as follows:

- (1) There are two distinct difficulties that confront modelers:
 - (a) the fluid trapped in a joint appears to be very stiff, owing to the small aperture; and
 - (b) permeability varies rapidly with changing aperture, owing to the cubic term in the flow equation.

The two difficulties are separate and can be addressed individually: for example, if the imposed pressure changes are small compared to the existing pressures (and rock stresses), then item (b) is unimportant.

- (2) It is rock, rather than the fluid, that determines fluid pressure. In a conventional pipe network, for example, the fluid determines its own pressure, via the flow and continuity equations. However, a typical rock block is so soft compared to the fluid trapped in a joint (factors of 10^3 to 10^4 are common) that significant changes in fluid volume hardly affect rock stresses. Since the rock's normal stresses must balance the fluid pressure in the neighboring joints, the fluid pressure is determined by the rock stress. It then follows that spatial variations in rock stress are directly responsible for the direction and magnitude of flow since flow occurs in response to pressure gradients.
- (3) If the interest is in unsteady (but not dynamic) flow; i.e., the model must accurately capture the transmission delay as pressure fluctuations migrate from one part of the system to another, then inertial effects or wave propagation effects can be neglected. We confine our attention to a liquid, such as water,

11/29

AT EACH FLUID TIMESTEP i

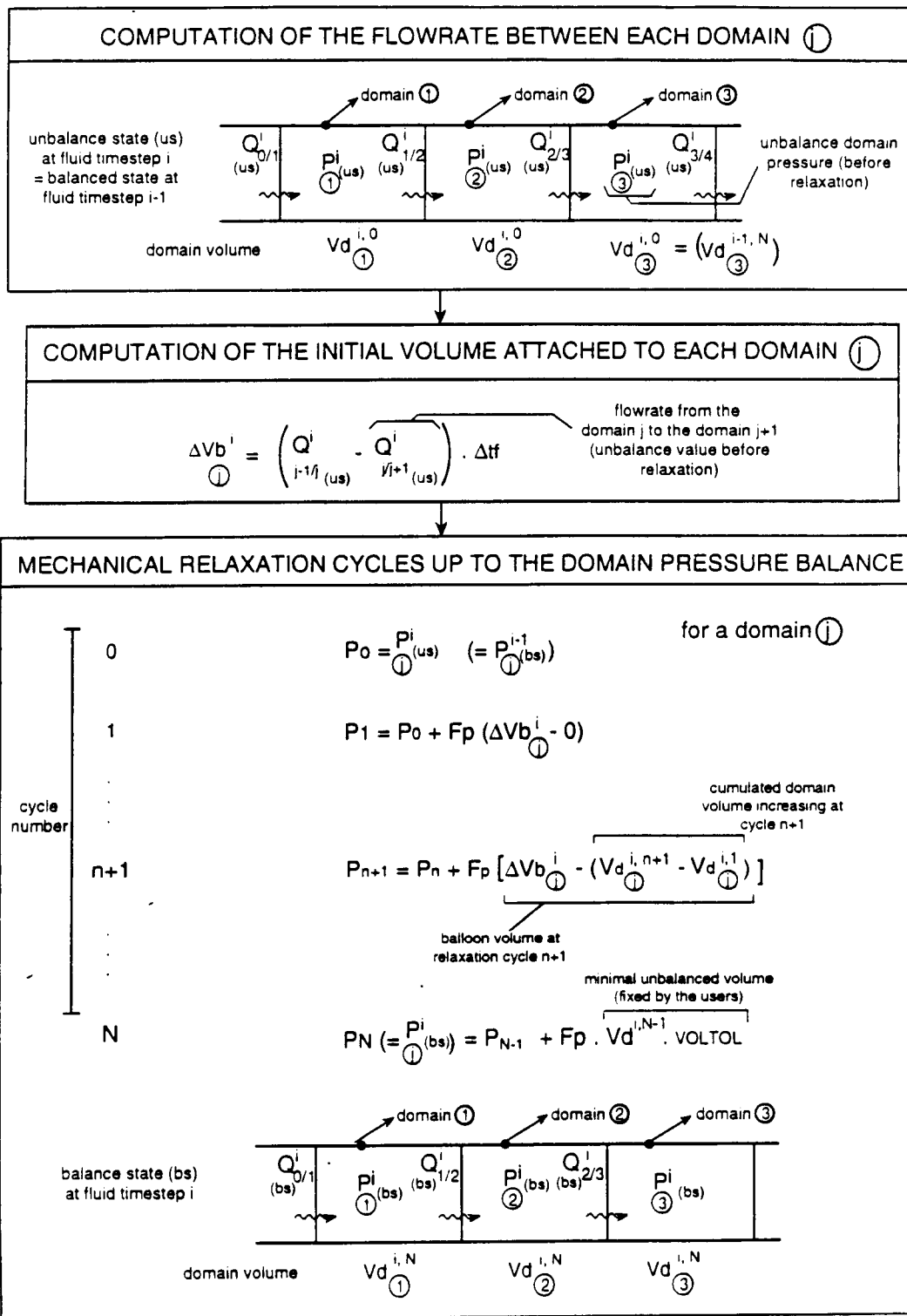


Figure 7.9. Transient hydro-mechanical scheme computation algorithm for each fluid cycle.

AT EACH RELAXATION CYCLE
(for example at cycle n)

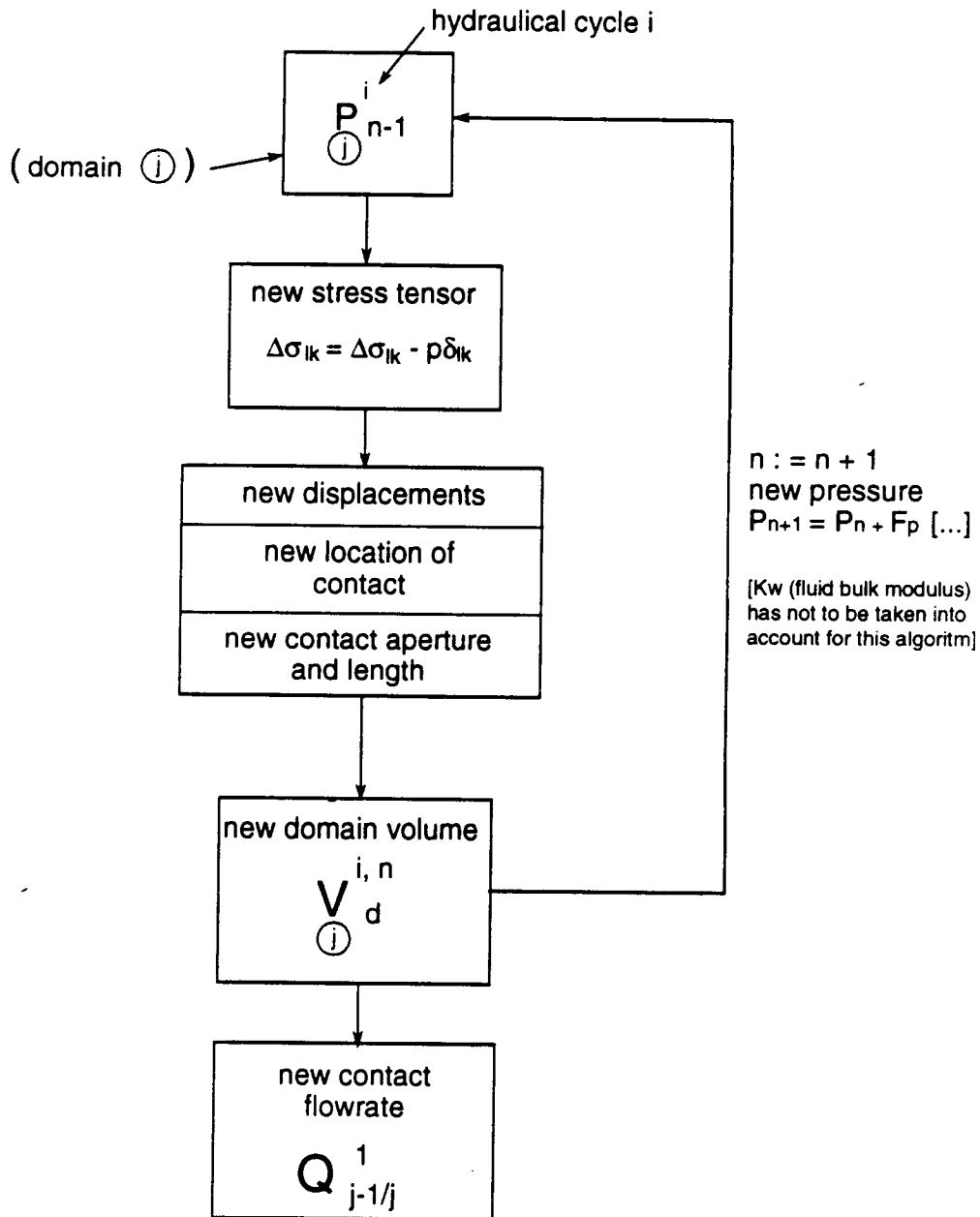


Figure 7.10. Transient hydro-mechanical scheme computation algorithm for each relaxation cycle.

7.3.3.3 Procedures for Introducing Thermal Convection into UDEC

7.3.3.3.1 Data Structure Modifications

UDEC requires data of different types. A distinction is made between those related to the blocks: the nodes and corners (nodes at the boundary of the blocks) and those related to the joints: the contacts (corner/corner c-c: between 2 corners, corner/edge c-e: between a corner and an edge) and the domains (located between two or more contacts). Figure 7.12 shows the representation of notation used in UDEC (Version 1.8).

In order to discretize Eq. (7.50) through (7.53), the case of a domain defined between two contacts shall be taken where each contact is defined between two corners (in the case of contacts of the corner/edge or edge/corner type. An additional corner on the edge where there is no corner shall be created. To simplify the problem, the domains involving more than three contacts (areas of intersections between the joints) have (temporarily) been set aside. Consider a domain, *i*, of length *d_i*, defined by the two contacts *K_{1,i}* and *K_{2,i}* where the hydraulic apertures of the joint are *a_{1,i}* and *a_{2,i}* respectively. The contact *K_{1,i}* is located between corners *C_{1,i}* and *C'_{1,i}* while *K_{2,i}* is located between *C_{2,i}* and *C'_{2,i}* (Figure 7-13). For each domain, *i*, a heat transfer coefficient *h_i*, a temperature *T_i^f*, and a velocity *v_i* equal to the mean of two velocities calculated in the two sections of the two contacts defining the domain shall be assigned.

7.3.3.3.2 Assumptions

For introducing thermal convection into UDEC, two assumptions have been made:

- Since it can be assumed that the longitudinal temperature gradient is low compared with the lateral gradient for fractures whose thicknesses are small compared with their lengths, the conductive heat transfer term between the two surfaces AB and CD can be neglected (Figure 7-11). The heat balance expressed in Eq. (7.53) becomes:

$$mC_p^f \frac{dT^f}{dt} = dQ_1 + dQ_3 + dQ'_3 \tag{7.54}$$

- The convective heat transfer is neglected for domains defined at joint intersections. This has been assumed because of the very small areas of those domains.

7.3.3.3.3 Discretization of the Heat Transfer Terms

Discretizing all the terms in the heat balance gives the following expressions:

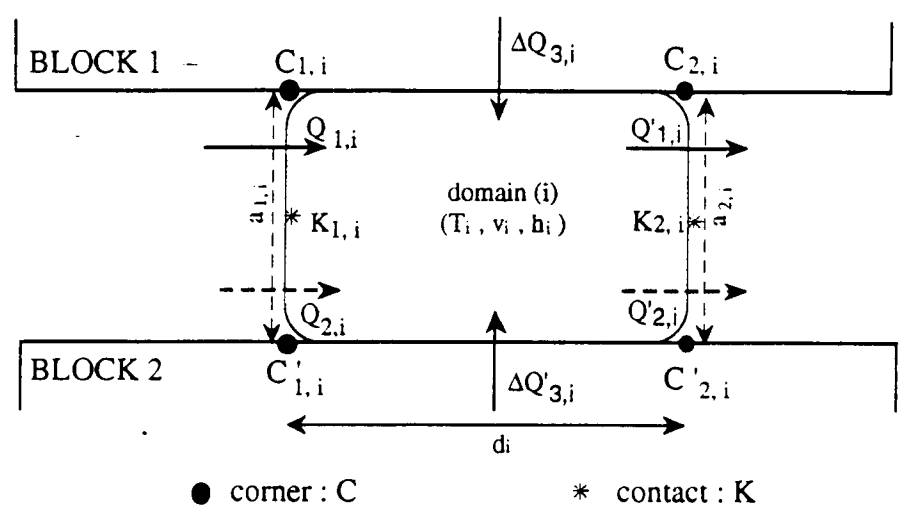


Figure 7.13. Discretization of the heat transfer at the interfaces of a domain in UDEC.

$$m_i C_p^f \frac{\Delta T_i^f}{\Delta t} = \Delta Q_{1,i} + \Delta Q_{3,i} + \Delta Q'_{3,i} \tag{7.59}$$

When replacing each term by its value, we obtain the expression for the change in the temperature in a domain, i, during a time step Δt :

$$\Delta T_i^f = \left[\frac{2h_i}{\rho_f a_i C_p^f} \left(\frac{T_{C_{1,i}} + T_{C_{2,i}} + T_{C'_{1,i}} + T_{C'_{2,i}}}{4} - T_i^f \right) - \left(v_i \left(\frac{T_i^f - T_{i-1}^f}{d_i} \right) + T_i^f \left(\frac{v_{k_{2,i}} - v_{k_{1,i}}}{d_i} \right) \right) \right] \Delta t \tag{7.60}$$

The temperature change in a corner related to a domain is given, here for example for corner $C_{1,i}$, by the following expression (already introduced into the UDEC code to model forced convection as a boundary condition):

$$\Delta T_{C_{1,i}} = h_i \left(\frac{d_i}{2} \right) (T_i^f - T_{C_{1,i}}) thm_{C_{1,i}} \Delta t \tag{7.61}$$

where $thm_{C_{1,i}}$ is the thermal capacity of the corner $C_{1,i}$ given as

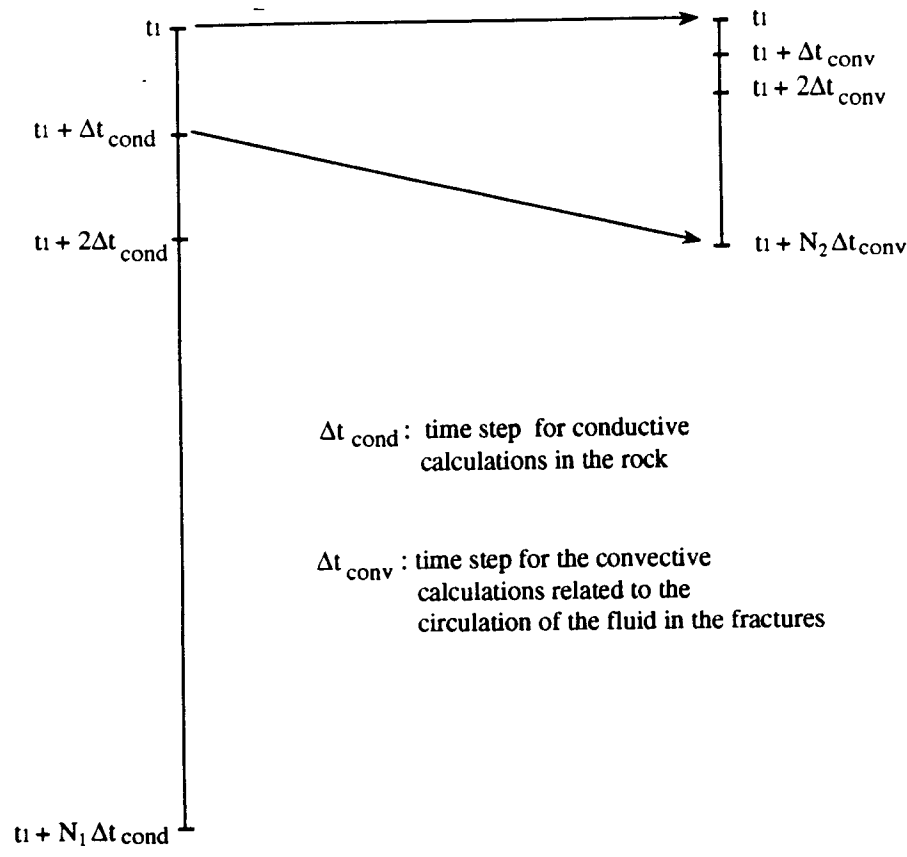


Figure 7.14. Conductive and convection timestep.

- $C_p^r = 900 \text{ J/kg} \cdot \text{K},$
- $C_p^f = 4200 \text{ J/kg} \cdot \text{K},$
- $a = 10^{-3} \text{ m},$
- $\rho^r = 2760 \text{ kg/m}^3$
- $\rho^f = 1000 \text{ kg/m}^3,$
- $\nu = 2.778 \times 10^{-4} \text{ Pa} \cdot \text{s}, \text{ so } \nu = 2.778 \times 10^{-7} \text{ m}^2/\text{s}$

The initial temperatures of the rock and fluid are zero. The boundary conditions are shown in Figure 7.16. A temperature difference of 100 °C and a pressure difference (for the fluid) of Δp (10 MPa in the base case) are imposed between the left-hand and right-hand edges of the model.

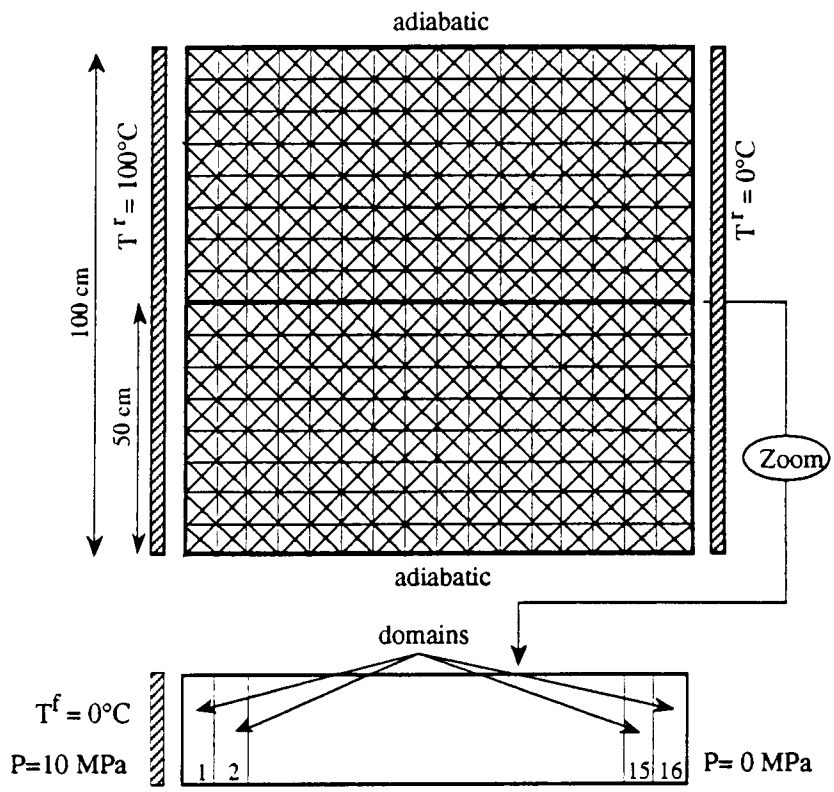


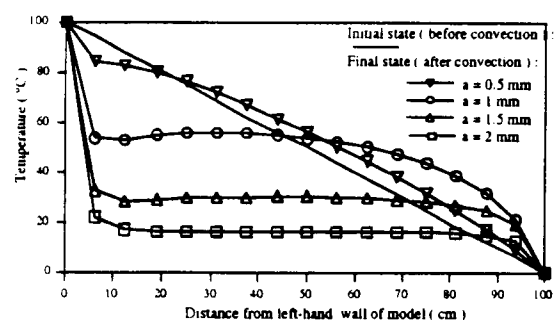
Figure 7.16. Model geometry, mesh, and boundary conditions (545 nodes, 1024 elements, 16 domains).

Comparison of Figures 7.17(a) and 7.17(b) clearly shows the importance of thermal convection: the isotherms are no longer lines perpendicular to the fracture surface, and they are especially distorted in the vicinity of the fracture. They show the presence of two zones in the rock:

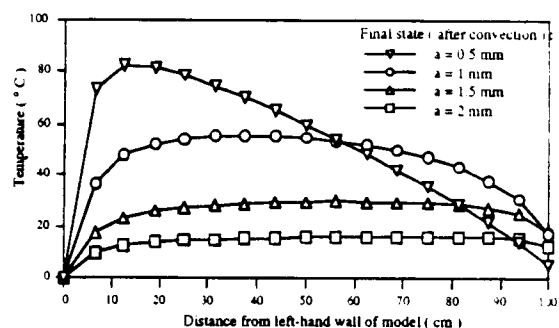
- a zone of cooling: the fluid circulates, cooling the rock which releases its heat.
- a zone of heating: after flowing over a certain distance, the fluid provides the rock the heat stored in the first zone.

7.3.3.4.3 Convection Sensitivity to Hydraulic Aperture, Flow Velocity, Fluid Viscosity

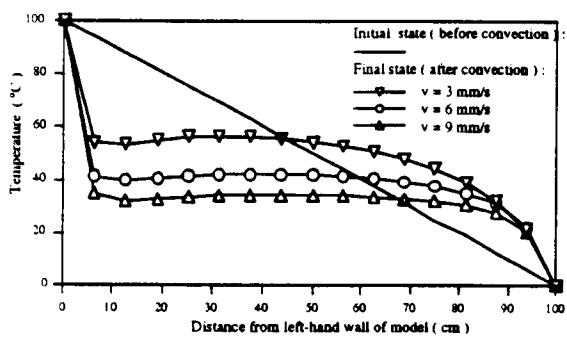
The importance of the hydraulic aperture, a , was investigated for four cases ($a = 0.5; 1; 1.5; \text{ and } 2 \text{ mm}$). Figure 7.18a shows the temperature profile in the rock along the fracture in the different cases, and Figure 7.18b shows that of the fluid circulating along the fracture.



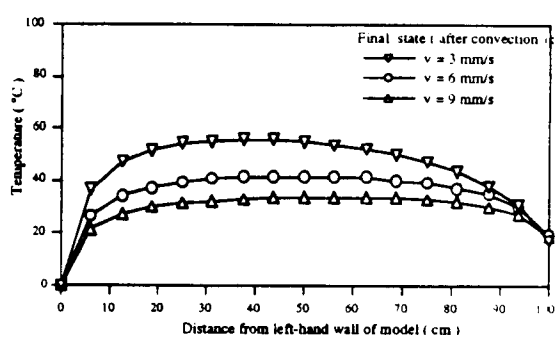
a - Effect of the hydraulic aperture on the temperature profile in the rock near the fracture



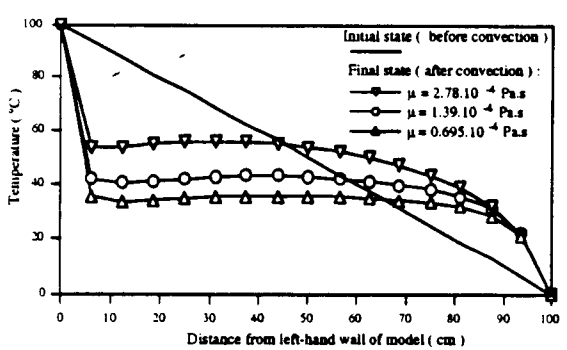
b - Effect of the hydraulic aperture on the temperature profile in the fluid along the fracture



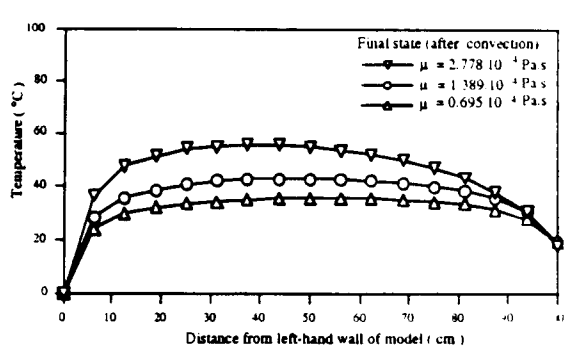
c - Effect of the fluid velocity on the temperature profile in the rock near the fracture



d - Effect of the fluid velocity on the temperature profile in the fluid along the fracture



e - Effect of the fluid viscosity on the temperature profile in the rock near the fracture



f - Effect of the fluid viscosity on the temperature profile in the fluid along the fracture

Figure 7.18. Effect of hydraulic aperture, fluid velocity, and fluid viscosity on temperature profiles.

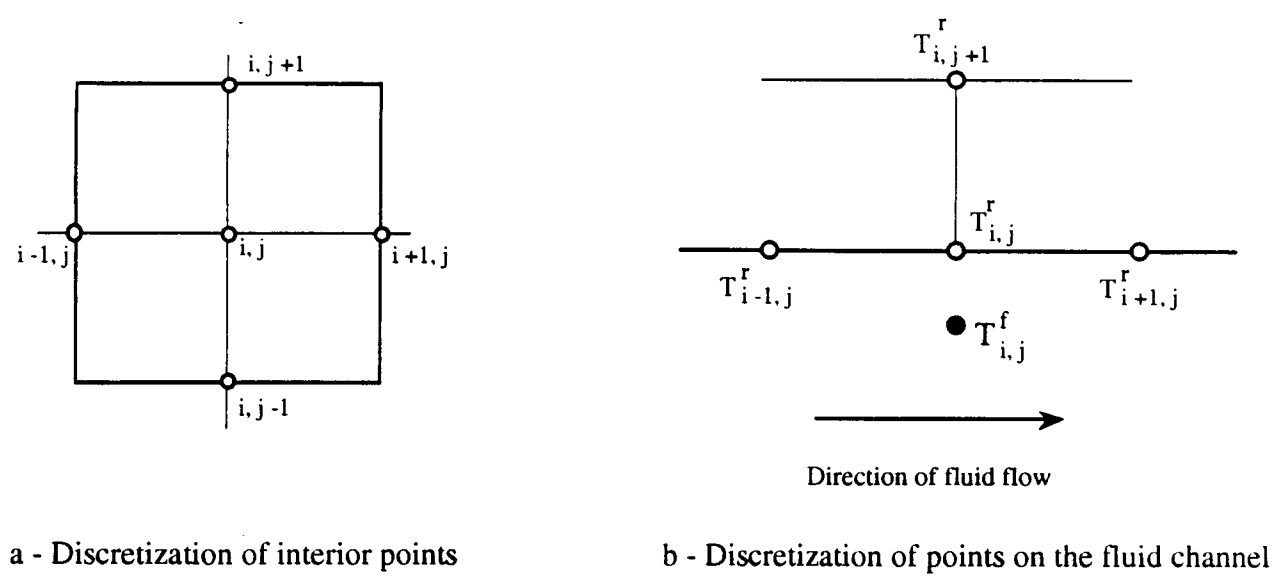


Figure 7.19. Discretization with a Finite Difference Scheme (FDS).

MATHEMATICA). This may be caused by the limited lateral dimension (normal to the fracture) of the rock, between the top and the bottom, where adiabatic boundary conditions are applied.

7.3.3.5 Estimation of the Importance of the Coupling Between Thermics and Hydromechanics

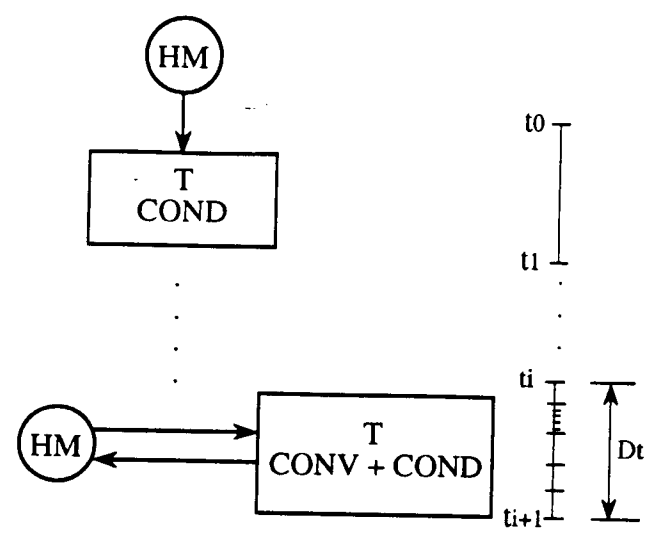
In the previous section the consistency of the model for thermo-hydrological computation was tested. The thermo-hydro-mechanical computation is now realized, allowing the hydraulic aperture to vary with the block strain.

The computation algorithm is depicted in Figure 7.21a. After realizing at first successively a HM computation followed by a T conductive computation, HM computations (using the steady-state algorithm) and T sequences (using the conductive/convective algorithm depicted in Figure 7.15) are alternated.

The realism of THM coupling simulations depends on the alternation number between HM and T calculations. The effect of thermal sequence duration Dt on the calculation (Dt is related to the thermal timesteps as follows: $Dt = N_1 \Delta t_{cond} = N_1 N_2 \Delta t_{conv}$) was analyzed. Changing the sequence duration Dt it can be seen in Figure 7.21b that:

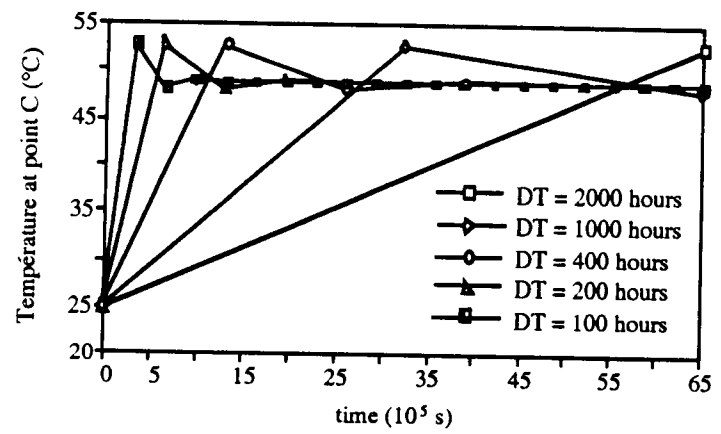
- long thermal sequences (up to 1,000 hours) are acceptable for steady-state analysis,

a - Computation algorithm

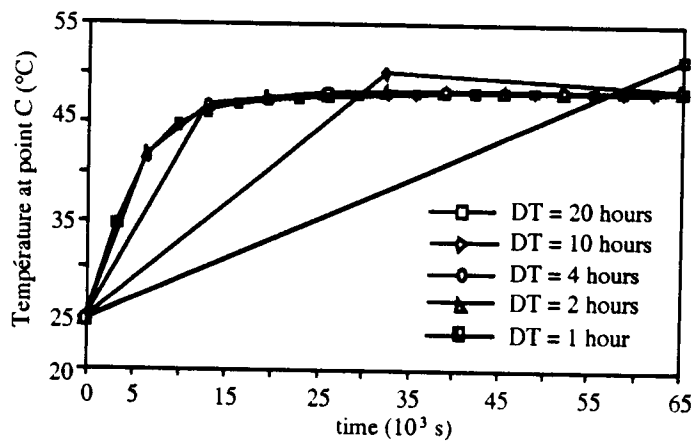


$Dt : \text{thermal sequence duration} = N1 \cdot \Delta t_{\text{cond}} = N1 \cdot N2 \cdot \Delta t_{\text{conv}}$

b - Results of the computations



long thermal sequences
(low coupling)
used for steady state
analysis



short thermal sequences
(strong coupling)
used for transient
analysis

Figure 7.21. Estimation of the importance of the coupling between thermics and hydromechanics.

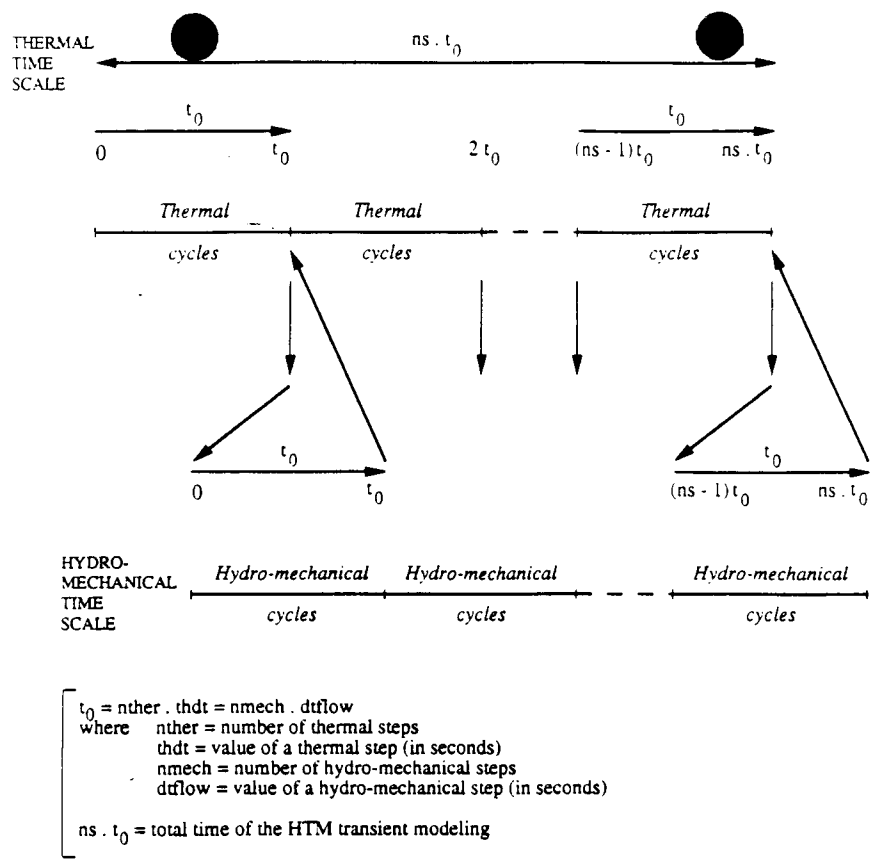


Figure 7.24. TMH process in UDEC with the transient HM analysis.

7.3.4.2 Approaches Toward Simplification of Complex Fracture Networks

The difficulty in the DEM arises when explicitly modeling a fractured rock mass with a very large number of fractures, which exist in more or less a randomly oriented distribution (i.e., no dominant joint sets exist). Although large numbers of fractures can be modeled with UDEC, when coupling the mechanical behavior with the thermal and hydrologic behavior of the system computational times can become exceedingly lengthy and impractical for standard engineering analyses. Simplifications to the fracture network are thus necessary in which one attempts to take into account only those fractures that are most important which, depending on the approach, could be those fractures that are the longest, most open, or most connected. The relevance of such simplifications is discussed in the following paragraphs.

In the case of Bench Mark Test 3 (BMT3), which is discussed in greater depth in Chapter 12, various modeling teams of DECOVALEX took different DEM approaches to simplify the 50×50-m domain containing approximately 6580 individual fractures. In the case of one modeling team (INERIS), two distinct geometries were chosen for the UDEC simulation. For the first one, all the fractures within a 20×20-m window around the origin of the BMT3 domain were included (Figure 7.25a). In the second model, only fractures with a hydraulic aperture greater than 3.0 μm within this same subdomain were chosen (Figure 7.25b). The characteristics used for the two calculations are presented in Table 7.1, and the results obtained from each UDEC analysis are given in Table 7.2. The results in Table 7.2 tend to indicate that the simplification is acceptable far from the gallery, but questionable

when close to it. Indeed, one can notice the high variation of the flowrate into the gallery or of the maximum displacement depending on the fracture geometry chosen.

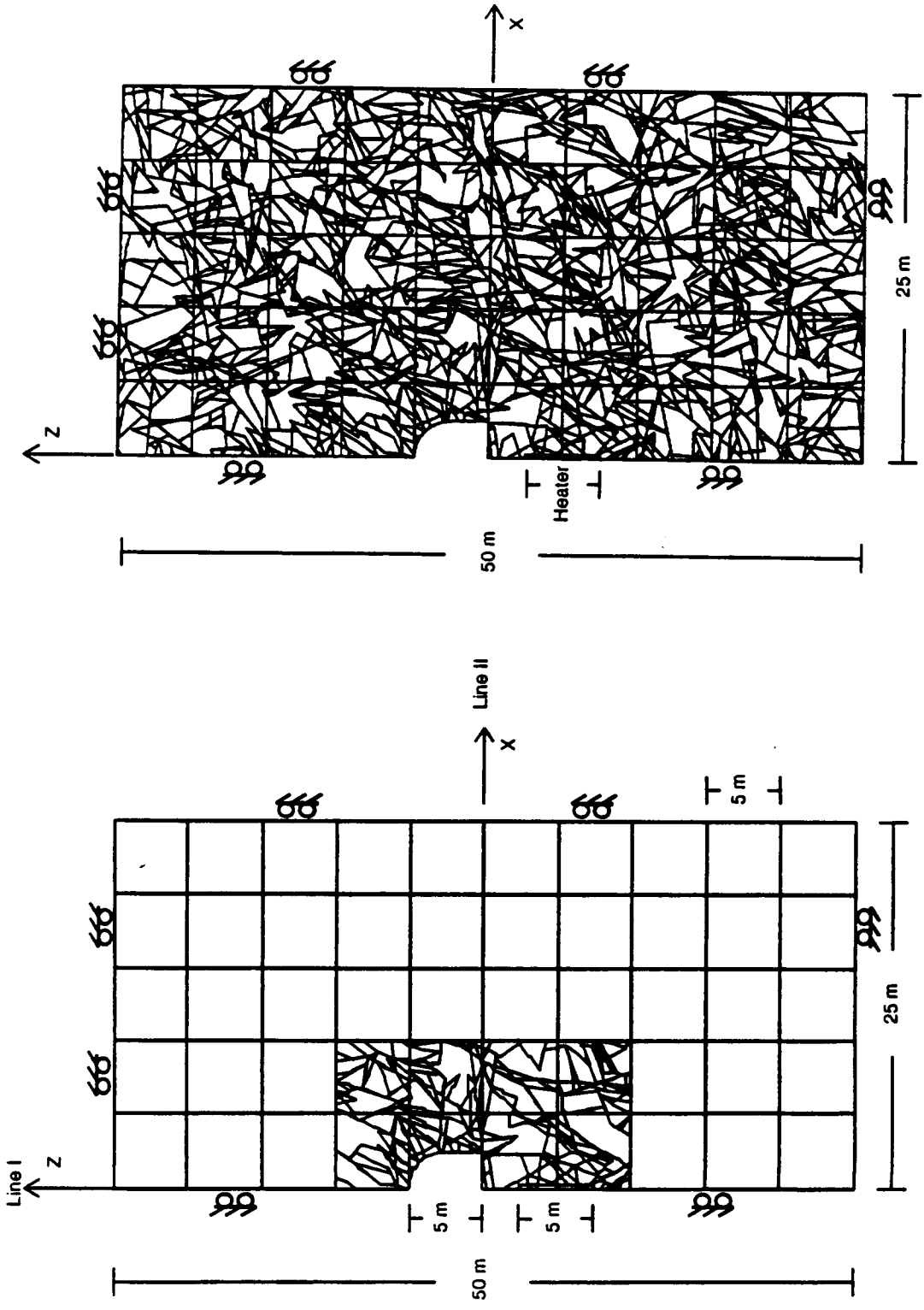
A slightly different simplification approach was taken by one of the other DECOVALEX modeling teams (CNWRA) in analyzing BMT3 using UDEC. In this approach, the fracture network was simplified based on fracture length rather than fracture aperture. Two geometries were analyzed as shown in Figure 7.26. Both cases assumed vertical symmetry about the vertical z plane, which was somewhat justified by the problem geometry and random nature of the fracture distribution, resulting in equivalent permeabilites in both the x and z directions for the entire domain being approximately equal. Case A shown in Figure 7.26a, consisted of an inner region (0.0 ≤ x ≤ 10.0 m, -10.0 ≤ z ≤ 10.0 m) containing all fractures from the original fracture network greater than 2.0 m in length. The remaining outer region (10.0 ≤ x ≤ 25.0 m, 10.0 ≤ |z| ≤ 25.0 m) shown in Figure 7.26b was modeled using an equivalent set of uniformly spaced joints to reduce the overall number of fractures, but still allow hydraulic connectivity between the outer boundaries with specified fluid pressure and the inner tunnel region. The spacing of the joints within the outer region was arbitrarily set, however assumptions were made regarding the appropriate aperture to assign these regularly spaced joints to maintain the same equivalent global permeability in the x and z directions. For a system of joints with spacing S, the average permeability for an equivalent continuum can be derived as (Itasca, 1992)

$$k = \frac{\rho_w g}{12\mu} \frac{a^3}{S} \tag{7.67}$$

- where k = permeability of equivalent continuum (m/s)
- ρ_w = density of water (kg/m³)
- μ = dynamic viscosity (N-s/m²)
- a = aperture (m)

Table 7.1. Characteristics of the 2 INERIS models studied for the sequence 2 of BMT3

Model	Fracture aperture threshold (microns)	Number of Fractures in the region A	Number of Gridpoints	Number of intersections with the tunnel	Number of calculation cycles
a	0	1,003	19,945	49	8,000,000
b	3	564	15,377	21	325,000



(a) UDEC models from CNWRA analysis of BMT3 showing distinct element blocks for (a) Case A and (b) Case B. (b)

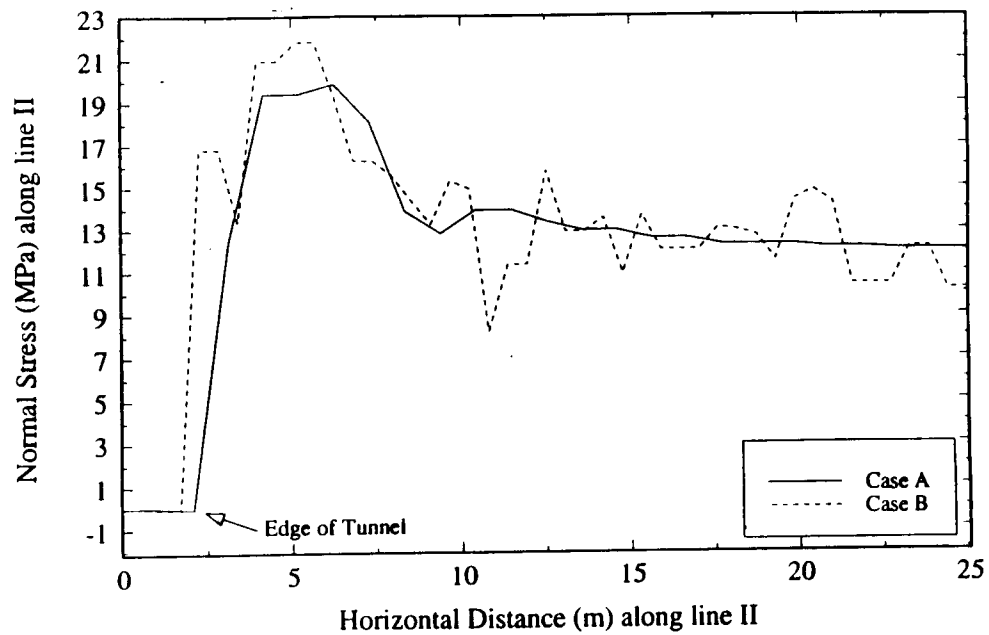


Figure 7.27b. Comparison of normal stresses along horizontal line II (i.e., σ_{yy}) for the two CNWRA UDEC cases after 4 yrs of heating.

7.4 REFERENCES

Abdallah, G., A. Thoraval, A. Sfeir, and J.P. Piguet, "Thermal Convection of Flow in Fractured Media," *International Journal of Rock Mechanics and Mining Sciences & Geomechanics Abstracts*, in publication.

Applied Mechanics Inc., "Use and Modification of the Universal Distinct Element Code (UDEC) for Basalt Block Test Analysis," SD-BWI-TD-020, Rev. 0, for Rockwell Hanford Operations, Richland, Washington, 1985.

Barton, N.R., and S.C. Bandis, "Effects of block size on the shear behavior of jointed rock," *Proceedings of the 23rd U.S. Symposium on Rock Mechanics*, Berkeley, California, 1982.

Barton, N.R., S.C. Bandis, and K. Bakhtar, eds., "Strength, deformation and conductivity coupling of rock joints," *International Journal of Rock Mechanics and Mining Sciences & Geomechanics Abstracts*, 22(3):121-140.

Battelle Memorial Institute, "Modelling Rock Joint Behavior from *In Situ* Block Tests. Implications for Nuclear Waste Repository Design," N. Barton, ONWI-308, Columbus, Ohio, 1982.

Center for Nuclear Waste Regulatory Analyses, "Field Site Investigation: Effect of Mine Seismicity on a Jointed Rock Mass," CNWRA 92-012, San Antonio, Texas, 1992.

- Itasca Consulting Group, Inc., "UDEC Universal Distinct Element Code Version 1.8 Volume I: User's Manual," Minneapolis, Minnesota, 1992.
- Jaeger, J.C., and N.G.W. Cook, *Fundamentals of Rock Mechanics*, 3rd Edition, Chapman and Hall, Ltd., London, United Kingdom, 1979.
- Karlekar, B.V., and R.M. Desmond, *Heat Transfer*, 2nd edition, West Publishing Co., St. Paul, Minnesota, 1982.
- Makurat, A., N. Barton, G. Vik, P. Chryssanthakis, and K. Monsen, "Jointed Rock Mass Modelling," N. Barton and O. Stephansson, eds. *Proceedings of the International Symposium on Rock Joints*, 647-656, A.A. Balkema, Rotterdam, Netherlands, 1990.
- Nitao, J.J., T.A. Buscheck, and D.A. Chestnut, "The implications of episodic non equilibrium fracture-matrix flow on site suitability and total system performance," *Proceedings of the International High-Level Radioactive Waste Management Conference*, 279-296, ANSI, La Grange Park, Illinois, 1992.
- Nuclear Regulatory Commission, "An Appraisal of Nuclear Waste Isolation in the Vadose Zone in Arid and Semi-arid Regions," H.A. Wollenberg, J.S.Y. Yang, and G. Korbin, NUREG/CR-3158, Washington, D.C. 1983.
- Nuclear Regulatory Commission Tsang. 1983. "Thermal Impact of Waste Emplacement and Surface Cooling Associated with Geologic Disposal of Nuclear Waste," J.S.Y. Wang, D.C. Mangold, R.K. Spencer, and C.F. Tsang, NUREG/CR-2910, Washington, D.C., 1983.
- Nuclear Regulatory Commission, "UDEC (Universal Distinct Element Code) Version ICGI.5," Vols. 1-3, NUREG/CR-5429, Washington, D.C., 1989.
- Nuclear Regulatory Commission, "Critical Assessment of Seismic and Geomechanics Literature Related to a High-Level Nuclear Waste Underground Repository," D.D. Kana, B.H.G. Brady, B.W. Vanzant, and P.K. Nair, NUREG/CR-5440, Washington, D.C. 1991.
- Nuclear Regulatory Commission, "A Literature Review of Coupled Thermal-Hydrologic-Mechanical-Chemical Processes Pertinent to the Proposed High-Level Nuclear Waste Repository at Yucca Mountain," R.D. Manteufel, M.P. Ahola, D.R. Turner, and A.H. Chowdhury, NUREG/CR-6021, Washington, D.C., 1993.
- Patankar, S.V., *Numerical Heat Transfer and Fluid Flow*, Hemisphere, Washington, D.C., 1980.
- Peter Cundall Associates; Contract DAJA37-79-C-0548, "UDEC - A Generalized Distinct Element Program for Modeling Jointed Rock," Report PCAR-1-80, European Research Office, U.S. Army, 1980.
- Sandford, T.C., E.R. Decker, and K.H. Maxwell, "The Effect of Discontinuities, Stress Level, and Discontinuity Roughness on the Thermal Conductivity of a Maine